Ion-gel-gating-induced oxygen vacancy formation in epitaxial La_{0.5}Sr_{0.5}CoO_{3−δ} films from in operando x-ray and neutron scattering

Jeff Walter, Guichuan Yu, Biqiong Yu, Alexander Grutter, Brian Kirby, Julie Borchers, Zhan Zhang, Hua Zhou, Turan Birol, Martin Greven, and Chris Leighton

Ion-Gel-Gating-Induced Oxygen Vacancy Formation in Epitaxial La$_{0.5}$Sr$_{0.5}$CoO$_{3-\delta}$ Films from *in operando* X-ray and Neutron Scattering

Jeff Walter,[1] Guichuan Yu,[2] Biqiong Yu,[2] Alexander Grutter,[3] Brian Kirby,[3] Julie Borchers,[3] Zhan Zhang,[4] Hua Zhou,[4] Turan Birol,[1] Martin Greven,[2] and Chris Leighton[1]*

[1]*Department of Chemical Engineering and Materials Science, University of Minnesota, Minneapolis, MN 55455*

[2]*School of Physics and Astronomy, University of Minnesota, Minneapolis, MN 55455*

[3]*NIST Center for Neutron Research, National Institute of Standards and Technology, Gaithersburg, MD 20899*

[4]*Advanced Photon Source, Argonne National Laboratory, Argonne, IL 60439*

Abstract: Ionic-liquid/gel-based transistors have emerged as a potentially ideal means to accumulate high charge carrier densities at the surfaces of materials such as oxides, enabling control over electronic phase transitions. Substantial gaps remain in the understanding of gating mechanisms however, particularly with respect to charge carrier *vs.* oxygen defect creation, one contributing factor being the dearth of experimental probes beyond electronic transport. Here we demonstrate the use of synchrotron hard X-ray diffraction and polarized neutron reflectometry as *in operando* probes of ion-gel transistors based on ferromagnetic La$_{0.5}$Sr$_{0.5}$CoO$_{3-\delta}$. An asymmetric gate bias response is confirmed to derive from electrostatic hole accumulation at negative gate bias *vs.* oxygen vacancy formation at positive bias. The latter is detected *via* a large gate-induced lattice expansion (up to 1 %), complementary bulk measurements and density functional calculations enabling *quantification* of the bias-dependent oxygen vacancy density. Remarkably, the gate-induced oxygen vacancies proliferate through the entire thickness of 30-40-unit-cell-thick films, quantitatively accounting for changes in the magnetization depth profile.

These results directly elucidate the issue of electrostatic *vs*. redox-based response in electrolyte-gated oxides, also demonstrating powerful new approaches to their *in operando* investigation.

*Corresponding author: leighton@umn.edu

SECTION: Magnetic, ferroelectric, and multiferroic materials

PHYSH: <u>Techniques</u>: X-ray diffraction, Neutron reflectometry

            <u>Physical Systems</u>: Field-effect transistors, Oxides

Electrolyte gating using ionic liquids and gels in electric double layer transistors (EDLTs) is emerging as a premier approach for the study and manipulation of carrier-density-controlled phenomena [1,2]. The nanoscopic EDL formed by the electrolyte cations (anions) and induced surface electrons (holes) results in very large capacitance (up to ~100 μF cm^{-2}) [3–5], inducing carrier densities exceeding 10^{14} cm^{-2} [4–9]. This is sufficient to control electronic and magnetic phase transitions [6–15], map phase behavior [12,13], and explore transport limits in semiconductors (*e.g.*, [4,5,13,16–19]). The electric fields in the EDLs are so large, however (~10 MV cm^{-1}), that mechanisms other than electrostatic carrier accumulation become possible. This is particularly important in transition metal oxides, where electrolyte gating is being extensively explored. Superconductivity was discovered, for instance, in electrolyte-gated KTaO$_3$ [6], and controlled in SrTiO$_3$ [10] and cuprates [11,12]. Metal-insulator transitions have been similarly controlled in VO$_2$ [14,20,21] and nickelates [7,15], while ferromagnetism has been modulated in Ti$_{1-x}$Co$_x$O$_2$ [8], La$_{1-x}$Sr$_x$MnO$_3$ [9], and La$_{1-x}$Sr$_x$CoO$_{3-\delta}$ [22]. It is increasingly apparent, however, that the gate response in oxides can be electrochemical rather than electrostatic, the electric field in the EDL inducing redox in the oxide, particularly *via* oxygen vacancy (V$_O$) formation. Evidence for bias-induced V$_O$ creation has been gathered from controlled atmosphere transport and tracer experiments in VO$_2$ [23], SrTiO$_3$ [24], and TiO$_2$ [25], although controversy remains, particularly in VO$_2$ [14,26].

Recent work of ours on ion-gel-gated La$_{0.5}$Sr$_{0.5}$CoO$_{3-\delta}$ (LSCO) films provided insight into this issue of electrostatics *vs.* electrochemistry by uncovering clear asymmetry with respect to gate bias (V_g) polarity [22]. While electrostatic hole accumulation was deduced at negative V_g in this *p*-type oxide, V$_O$ formation was implicated at positive V_g, from transport [22]. This was interpreted in terms of the known redox stability of LSCO, similar to many oxides, where V$_O$

creation is thermodynamically preferred to V_O annihilation. At positive V_g, V_O formation is thus favored over hole depletion, while at negative V_g hole accumulation is favored over V_O annihilation [22]. This could indicate that *n*-type oxides such as VO_2, which require EDLT operation at $V_g > 0$ (at least for undoped materials), could be particularly prone to V_O formation. Such explanations are attractive, but require further testing. In addition, recent work has placed further emphasis on V_g-induced ionic motion by uncovering electrochemical hydrogen incorporation in WO_3 [27] and $SrCoO_{2.5}$ [28]. There are thus several emerging control concepts in oxide EDLTs, further work being needed to untangle mechanisms.

One impediment to improved understanding of electrolyte gating is the dearth of available probes beyond electronic transport. The latter is dominant in the field, other more direct probes, such as spectroscopy and scattering, being challenging to implement in EDLTs. Difficulties include the small volume of gated material, and the thick overlying ion gel or ionic liquid, which induce absorption and scattering. Few demonstrations of *in operando* scattering or spectroscopy of electrolyte-gated oxides have thus appeared, although this now appears to be changing. Synchrotron X-ray diffraction (SXRD) results on ionic-liquid-gated VO_2 [26], $La_{2-x}Sr_xCuO_4$ [29], $SrCoO_{2.5}$ [28], WO_3 [27], and $NdNiO_3$ [30] have recently appeared, along with X-ray absorption on $YBa_2Cu_3O_{7-x}$ [31] and $NdNiO_3$ [30]. Noteworthy findings emerge from these studies, including giant V_g-induced lattice expansion in VO_2 [26], deoxygenation of $YBa_2Cu_3O_{7-x}$ under positive V_g [31], three-phase switching of $(H)SrCoO_{3-\delta}$ [28], and gate bias polarity asymmetry (similar to LSCO [22]) in $NdNiO_3$ [30]. *In operando* probes have thus yielded substantial insight, and additional work is clearly desirable, particularly with techniques capable of detecting V_O formation quantitatively, with spatial resolution.

In this work we demonstrate application of both SXRD and polarized neutron reflectometry (PNR) as *in operando* probes of epitaxial LSCO EDLTs, utilizing the penetration of hard X-rays and neutrons. SXRD reveals only a small (<0.1 %) decrease in the out-of-plane lattice parameter under negative V_g, compared to a large increase at positive V_g (up to 1 % at +2 V). Complementary bulk powder XRD (PXRD) and thermo-gravimetric analysis (TGA) confirm that such lattice expansion is consistent with V_O formation, reproduced by density functional theory (DFT). The cell volume dependence on oxygen deficiency is then used to "calibrate" *in operando* SXRD, enabling *quantification* of the V_g-dependent V_O density, which reaches δ = 0.16 at +2 V. Importantly, SXRD indicates that these V_Os proliferate through the entire thickness of ~30-unit-cell-thick films. This is confirmed by V_g-dependent PNR, the suppressed magnetization extending through the whole film, in *quantitative* agreement with the determined O deficiency. These results not only advance our understanding of gating mechanisms in oxide EDLTs, but demonstrate powerful new approaches to *in operando* structural and magnetic studies.

Details on film growth, device fabrication, *in operando* measurements, and bulk measurements/calculations are provided in Supplemental Material Sections A-E (Figs. S1-S3) [32]. Briefly, epitaxial LSCO was deposited on LaAlO₃(001) (LAO) using high-pressure oxygen sputtering [22] and then thoroughly characterized [33–36]. Bulk-like metallic ferromagnetism with Curie temperature, $T_C \approx$ 220 K was obtained above 7 unit cell thicknesses. EDLTs employing ~10-μm-thick "cut and stick" ion gels [3] (see Fig. 1(a)) were then fabricated from these films. SXRD (Fig. 1(a)) was performed on the 33-ID beamline of the Advanced Photon Source, with 20 keV (λ = 0.62 Å) radiation. Beam damage was reduced to negligible levels *via* procedures discussed in Supplemental Material Section B (Fig. S2) [32]. PNR was

performed on the Polarized Beam Reflectometer at the NIST Center for Neutron Research (Supplemental Material Section C [32]), using a monochromated (4.75 Å) neutron beam, at 30 K, in a saturating 3 T in-plane magnetic field (B), and refinement was done with Refl1D [37]. For both SXRD and PNR, devices were operated in vacuum (< 10^{-5} Torr), V_g being applied at 280-290 K for 30 min, with *in situ* monitoring of electrical transport. Complementary TGA in 1 atm of flowing N_2 was performed on *bulk* LSCO (Supplemental Material Section D [32]). DFT+U calculations were performed using the Vienna *ab initio* Simulation Package [38,39], using methods described in Supplemental Material Section E [32].

Starting with *in operando* SXRD, Fig. 1(b) displays specular 00L scans around the 002 LAO substrate reflection, at V_g = -3.5, -1, 0, 1 and 2 V. As shown in Supplemental Material Fig. S2(c) [32], no ion-gel-induced changes were observed prior to V_g application. The V_g = 0 scan is typical of LAO(001)/LSCO [35,40]: a well-defined LSCO peak occurs at L = 1.95, corresponding to out-of-plane lattice parameter c_{op} = 3.89 Å, surrounded by Laue oscillations. As expected for a fully-strained film with negligible microstrain (Supplemental Material Section A, Fig. S1 [32]), the Scherrer length from the film peak width (t_S = 103 ± 6 Å) and the thickness from the oscillation spacing (t_f = 109 ± 7 Å) are in agreement with the thickness from X-ray reflectometry prior to gel application (t = 110 ± 5 Å, *i.e.*, 28 unit cells). When gating is performed, negative V_g (*e.g.*, -1 or -3.5 V in Fig. 1(b)) results in only small changes in the 002 LSCO peak. For positive V_g, however, the situation is different: the LSCO reflection rapidly shifts to lower L, and the Laue oscillations become less prominent, indicating increased roughness/structural disorder. These changes are summarized in Fig. 1(c,d,e), which shows the V_g dependence of the c-axis lattice parameter shift (Δc_{op}), Scherrer length shift (Δt_S), and fringe spacing thickness shift (Δt_f). The right axes show the cell volume change (ΔV) and absolute t_S

6

and t_f, respectively. From Fig. 1(c), the asymmetry with respect to V_g polarity is striking. Negative V_g up to -3.5 V results in a c_{op} decrease of < 0.1% (roughly linear in V_g), whereas V_g = +2 V induces a large (non-linear) 1% lattice expansion. As shown in Figs.1(d,e), this shift in c_{op} is accompanied by barely any variation in t_S and t_f, the only evidence of a statistically significant change occurring in t_S at + 2 V (see Supplemental Material Section F [32] for further discussion). This indicates, as can be seen from Fig. 1(b), that the LSCO film peak and Laue oscillations are uniformly shifted to lower L at positive V_g, with no signficiant broadening or peak splitting. This suggests that the positive-bias-induced lattice expansion occurs through the entire thickness of these 28-unit-cell films. In these measurements, which were performed in vacuum, the increase in c_{op} at positive V_g is irreversible (Supplemental Material Section F, Fig. S4) [32].

As discussed above, earlier transport studies on LSCO revealed similarly asymmetric V_g response, ascribed to V_O formation at positive bias, and electrostatic hole accumulation at negative bias [22]. V_O formation is thus an obvious possibility for the positive-bias-induced lattice expansion in Fig. 1(c). To investigate the cell volume - V_O density relationship in LSCO, *bulk* samples were systematically reduced in a TGA apparatus in flowing N_2. After each reduction these samples were then studied by PXRD. The PXRD pattern of the initial LSCO (bottom of Fig. 2(a)) is consistent with expectations for Pm$\bar{3}$m LSCO (Fig. 2(b)) [41]. As justified by the synthesis conditions and measured magnetic properties (Supplemental Material Section D [35]), we label this sample "$\delta = 0$" in Fig. 2(a), *i.e.*, we assume an initial state with negligible V_O density. The progressive reduction cycles shown in Fig. 2(c), to maximum temperatures from 340 - 1000 °C, result in mass loss that can be directly converted to δ. The PXRD patterns in Fig. 2(a) are thereby labeled with a deduced δ, increasing towards the top. The

cubic perovskite structure is retained up to $\delta = 0.202$, above which secondary phases form, being

LSCO reduction products (brownmillerite, binary oxides, *etc.*).

As shown in Fig. 2(d), which plots the cubic lattice parameter (*a*) and cell volume

expansion (ΔV) *vs.* δ, the reduction of bulk LSCO is indeed accompanied by lattice expansion,

qualitatively consistent with prior work [42–44]. ΔV increases linearly with V_O concentration, at

a rate that can be reproduced by DFT. Specifically, as detailed in Supplemental Material Section

E (Fig. S3, Table S1) [32] incorporation of V_Os in DFT supercells at various concentrations

results in the solid lines shown in Fig. 2(d) for Co U values (U_{Co}) of 5 and 6 eV. A U_{Co} between

these values, which is reasonable for Co perovskites [45], thus quantitatively reproduces the

experimental $\Delta V(\delta)$. Taken with the earlier indirect conclusion of V_O formation from transport,

and the observation of irreversibility in vacuum that is suppressed in O_2 (Supplemental Material

Section F [32]), we take these results as strong evidence for V_O formation as the source of lattice

expansion at positive V_g in Fig. 1(c). Importantly, this $\Delta V(\delta)$ relationship for bulk LSCO can then

be used in conjunction with the $\Delta V(V_g)$ relationship for gated films to quantitatively estimate the

change in δ induced by V_g. This essentially uses the bulk data of Fig. 2(d) as a calibration to

quantify $\delta(V_g)$ from Fig. 1(c), assuming the cell expansion with δ to be similar in films and bulk.

The straight line fit in Fig. 2(d) was used for this purpose, resulting in Fig. 2(e). Here, we simply

plot $\Delta\delta$, the V_g-induced change in δ with respect to zero bias, as the initial δ in these films is not

accurately known [46]. [As outlined in Supplemental Material Section G (Fig. S5) [32], the

Poisson ratio can also be accounted for in this analysis, assuming isotropic linear elasticity; this

modifies the absolute values in Fig. 2(e) but not the qualitative trend]. The resulting induced δ's

at positive V_g are large but reasonable, reaching 0.16 at 2 V. Note here that: (*a*) $\delta < 0.5$ even at

the largest positive V_g is consistent with the absence of brownmillerite in SXRD, and (*b*) strong

arguments can be made against a H incorporation mechanism (Supplemental Material Section H [32]). While the interpretation of the large structural changes at $V_g > 0$ are thus clear, the small ones occurring at $V_g < 0$ could involve both electrochemistry and electrostatics (Supplemental Material Section I, Table S2 [32]).

Clearly, a key conclusion from the above is that bias-induced V_O's appear to penetrate the entire film thickness. To verify this, a depth-sensitive technique, neutron reflectometry, was applied. Although V_O formation at the densities in Fig. 2(e) results in nuclear scattering length density changes that are difficult to discern (Supplemental Material Section J (Tables S3, S4) [32]), the subsequent impact on magnetization is substantial. Magnetization depth profiling *via* PNR was thus performed, using devices scaled to 10×5 mm^2 LSCO channels (Fig. 3(a)). Figure 3(b) shows the scattering vector (Q) dependence of the specular neutron reflectivity for 42-unit-cell-thick LSCO, at 30 K in a 3 T in-plane field [47] at $V_g = 0$. The non-spin-flip reflectivities ("R^{++}" and "R^{--}") are shown, where "+" and "−" indicate the polarization of the incoming and outgoing beams (Fig. 3(a)). As expected, well below T_C in a large in-plane field, R^{++} and R^{--} are clearly split. Fig. 3(c) plots the spin asymmetry, SA = $\left(\frac{R^{++}-R^{--}}{R^{++}+R^{--}}\right)$, which, in the absence of large V_G-dependent chemical changes, highlights the magnetic scattering. This SA is positive, with two oscillations visible to the maximum Q. Most significantly, Fig. 3(d,e) shows that the SA responds dramatically to V_g. The SA is reduced substantially at 2 V, but with a similar oscillation period, while at 3 V the SA appears completely suppressed. Even prior to quantitative analysis, this SA reduction with V_g indicates strong suppression of the magnetization, the similarity of the period in Figs. 3(c,d) indicating little change in magnetic thickness, *i.e.*, relatively uniform suppression.

Quantitative refinement was performed to substantiate these conclusions, resulting in the solid line fits in Fig. 3(b,c,d,e). As discussed in Supplemental Material Section J [32], these fits are based on a model including the LAO substrate, LSCO film, and ion gel. The refined nuclear scattering length densitiy for LSCO is as expected, and independent of V_g (along with the chemical thickness). Note here that varying δ between $La_{0.5}Sr_{0.5}CoO_3$ and $La_{0.5}Sr_{0.5}CoO_{2.84}$ (as in Fig. 2(e)) results in nuclear scattering length density changes of only 3 %, confirming little sensitivity to this effect. The depth-dependent magnetization ($M(z)$), however, is highly sensitive to V_O density. The refined $M(z)$ from Fig. 3(b-e) is plotted in Fig. 3(f). At $V_g = 0$ a single ferromagnetic LSCO layer with $M = 1.68$ μ_B/Co describes the data (Fig. 3(b,c)), with roughnesses of 4 Å and 8 Å at the LAO/LSCO and LSCO/ion gel interfaces, respectively. 1.68 μ_B/Co is slightly lower than the bulk saturation magnetization (1.9 μ_B/Co), but is consistent with magnetometry on these films [47]. While a reasonable description of the 2 and 3 V data was also possible with a single ferromagnetic LSCO layer with progressively suppressed M, statistically significant fit improvements were obtained by introducing a second layer. This captures the weak dip to negative SA around 0.045 Å^{-1} in Fig. 3(d). The resulting $M(z)$ in Fig. 3(f) reveals strong suppression of M with increasing V_g. At 2 V, M is roughly cut in half, the region closest to the ion gel interface having a slightly stronger reduction than the bulk of the film. At 3 V, M then becomes very small, a weakly magnetized bottom section of the LSCO providing the fit in Fig. 3(e). These results not only confirm near-uniform magnetization suppression, but are also *quantitatively* consistent with the δs from SXRD. Explicitly, taking the depth-averaged $M(V_g)$ from Fig. 3(f), and using bulk data for the x dependence of saturation magnetization in $La_{1-x}Sr_xCoO_3$ [48], an effective doping level (x_{eff}) can be extracted at each V_g. Using the fact that Sr hole doping is compensated by V_Os according to $x_{eff} = x - 2\delta$ (assuming doubly ionized V_O

donors), the curves in Fig. 3(f) can then be associated with an induced δ. These values are 0.11 and 0.18 for $V_g = 2$ and 3 V, which, considering the approximations, are in reasonable agreement with Fig. 2(e). While this analysis ignores other factors in the relationship between M and δ, making it only approximate, such an approach has been employed before and independently verified [34].

Given that the electric field in EDLTs based on metallic perovskites should be screened over quite short scales (the Thomas-Fermi screening length is a few unit cells) the observation of gate-induced V_O formation through 40-unit-cell films warrants discussion. One interpretation is that V_O creation is first achieved by the EDL electric field at the extreme surface of LSCO. While the details remain to be understood, this would then generate an O chemical potential gradient, driving further out-migration of O from the bulk, potentially assisted by the electric field. Importantly, the V_O diffusivity in LSCO [49] is large enough to support this interpretation, translating to a V_O diffusion length of 35 nm at 300 K on the time scales used here, well in excess of the 17 nm film thickness. The enthalpy of formation of V_Os is also low in LSCO (as utilized in recent Gd gettering studies [50]) due to the instability of Co^{4+} formal valence. This results in extraordinary redox activity at $x = 1$, consistent with recent demonstrations of thermal [51] and electrolyte-assisted [28] switching between $SrCoO_{3-\delta}$ and brownmillerite $SrCoO_{2.5}$. The extent to which EDLT response in a given system involves redox is thus heavily influenced by the enthalpy of formation of V_Os, their diffusivity, and the V_g polarity.

In summary, we report the use of SXRD and PNR as *in operando* probes of gating mechanisms in ion-gel-based LSCO EDLTs. Large positive-bias-induced lattice expansion is observed, providing direct evidence of V_O formation. Complementary bulk measurements using TGA and PXRD, supported by DFT, are then used to quantify the V_g-dependent V_O density,

which reaches $\delta = 0.16$ at +2 V. This electrochemical reduction penetrates the entire thickness of ~30-unit-cell-thick films, confirmed by uniform suppression of the magnetization depth profile from PNR, quantitatively consistent with the deduced V_O density. The results thus establish SXRD and PNR as powerful *in operando* probes of electrolyte-gated materials, significantly advancing our understanding of gating mechanisms in oxide EDLTs.

REFERENCES

[1]   C. H. Ahn, A. Bhattacharya, M. Di Ventra, J. N. Eckstein, C. D. Frisbie, M. E. Gershenson, A. M. Goldman, I. H. Inoue, J. Mannhart, A. J. Millis, A. F. Morpurgo, D. Natelson, and J.-M. Triscone, Electrostatic modification of novel materials, Rev. Mod. Phys. **78**, 1185 (2006).

[2]   A. M. Goldman, Electrostatic gating of ultrathin films, Annu. Rev. Mater. Res. **44**, 45 (2014).

[3]   K. H. Lee, M. S. Kang, S. Zhang, Y. Gu, T. P. Lodge, and C. D. Frisbie, "Cut and stick" rubbery ion gels as high capacitance gate dielectrics, Adv. Mater. **24**, 4457 (2012).

[4]   W. Xie, X. Zhang, C. Leighton, and C. D. Frisbie, 2D insulator-metal transition in aerosol-jet-printed electrolyte-gated indium oxide thin film transistors, Adv. Electron. Mater. **3**, 1600369 (2017).

[5]   H. Yuan, H. Shimotani, A. Tsukazaki, A. Ohtomo, M. Kawasaki, and Y. Iwasa, High-density carrier accumulation in ZnO field-effect transistors gated by electric double layers of ionic liquids, Adv. Funct. Mater. **19**, 1046 (2009).

[6]   K. Ueno, S. Nakamura, H. Shimotani, H. T. Yuan, N. Kimura, T. Nojima, H. Aoki, Y. Iwasa, and M. Kawasaki, Discovery of superconductivity in $KTaO_3$ by electrostatic carrier doping, Nat. Nanotechnol. **6**, 408 (2011).

[7]   R. Scherwitzl, P. Zubko, I. G. Lezama, S. Ono, A. F. Morpurgo, G. Catalan, and J. M. Triscone, Electric-field control of the metal-insulator transition in ultrathin $NdNiO_3$ films, Adv. Mater. **22**, 5517 (2010).

[8]   Y. Yamada, K. Ueno, T. Fukumura, H. T. Yuan, H. Shimotani, Y. Iwasa, L. Gu, S. Tsukimoto, Y. Ikuhara, and M. Kawasaki, Electrically induced ferromagnetism at room

temperature in cobalt-doped titanium dioxide, Science **332**, 1065 (2011).

[9]   A. S. Dhoot, C. Israel, X. Moya, N. D. Mathur, and R. H. Friend, Large electric field

effect in electrolyte-gated manganites, Phys. Rev. Lett. **102**, 136402 (2009).

[10]   K. Ueno, S. Nakamura, H. Shimotani, A. Ohtomo, N. Kimura, T. Nojima, H. Aoki, Y.

Iwasa, and M. Kawasaki, Electric-field-induced superconductivity in an insulator, Nat.

Mater. **7**, 855 (2008).

[11]   A. T. Bollinger, G. Dubuis, J. Yoon, D. Pavuna, J. Misewich, and I. Božović,

Superconductor-insulator transition in $La_{2-x}Sr_xCuO_4$ at the pair quantum resistance, Nature

472, 458 (2011).

[12]   X. Leng, J. Garcia-Barriocanal, S. Bose, Y. Lee, and A. M. Goldman, Electrostatic control

of the evolution from a superconducting phase to an insulating phase in ultrathin

$YBa_2Cu_3O_{7-x}$ films, Phys. Rev. Lett. **107**, 27001 (2011).

[13]   J. Ye, Y. Zhang, R. Akashi, and M. Bahramy, Superconducting dome in a gate-tuned band

insulator, Science **338**, 1193 (2012).

[14]   M. Nakano, K. Shibuya, D. Okuyama, T. Hatano, S. Ono, M. Kawasaki, Y. Iwasa, and Y.

Tokura, Collective bulk carrier delocalization driven by electrostatic surface charge

accumulation., Nature **487**, 459 (2012).

[15]   S. Asanuma, P.-H. Xiang, H. Yamada, H. Sato, I. H. Inoue, H. Akoh, A. Sawa, K. Ueno,

H. Shimotani, H. Yuan, M. Kawasaki, and Y. Iwasa, Tuning of the metal-insulator

transition in electrolyte-gated $NdNiO_3$ thin films, Appl. Phys. Lett. **97**, 142110 (2010).

[16]   S. Wang, M. Ha, M. Manno, C. D. Frisbie, and C. Leighton, Hopping transport and the

Hall effect near the insulator-metal transition in electrochemically gated poly(3-

hexylthiophene) transistors, Nat. Commun. **3**, 1210 (2012).

[17] W. Xie, S. Wang, X. Zhang, C. Leighton, and C. D. Frisbie, High conductance 2D transport around the hall mobility peak in electrolyte-gated rubrene crystals, Phys. Rev. Lett. **113**, 1 (2014).

[18] J. Ye, M. F. Craciun, M. Koshino, S. Russo, S. Inoue, H. Yuan, H. Shimotani, A. F. Morpurgo, and Y. Iwasa, Accessing the transport properties of graphene and its multilayers at high carrier density, Proc. Natl. Acad. Sci. **108**, 13002 (2011).

[19] T. Yamaguchi, E. Watanabe, H. Osato, D. Tsuya, K. Deguchi, T. Watanabe, H. Takeya, Y. Takano, S. Kurihara, and H. Kawarada, Low-temperature transport properties of holes introduced by ionic liquid gating in hydrogen-terminated diamond surfaces, J. Phys. Soc. Japan **82**, 74718 (2013).

[20] H. Ji, J. Wei, and D. Natelson, Modulation of the electrical properties of VO_2 nanobeams using an ionic liquid as a gating medium, Nano Lett. **12**, 2988 (2012).

[21] Z. Yang, Y. Zhou, and S. Ramanathan, Studies on room-temperature electric-field effect in ionic-liquid gated VO_2 three-terminal devices, J. Appl. Phys. **111**, 14506 (2012).

[22] J. Walter, H. Wang, B. Luo, C. D. Frisbie, and C. Leighton, Electrostatic versus electrochemical doping and control of ferromagnetism in ion-gel-gated ultrathin $La_{0.5}Sr_{0.5}CoO_{3-\delta}$, ACS Nano **10**, 7799 (2016).

[23] J. Jeong, N. Aetukuri, T. Graf, T. D. Schladt, M. G. Samant, and S. S. P. Parkin, Suppression of metal-insulator transition in VO_2 by electric field-induced oxygen vacancy formation, Science **339**, 1402 (2013).

[24] M. Li, W. Han, X. Jiang, J. Jeong, M. G. Samant, and S. S. P. Parkin, Suppression of ionic liquid gate-induced metallization of $SrTiO_3(001)$ by oxygen, Nano Lett. **13**, 4675 (2013).

[25] T. D. Schladt, T. Graf, N. B. Aetukuri, M. Li, A. Fantini, X. Jiang, M. G. Samant, and S.

S. P. Parkin, Crystal-facet-dependent metallization in electrolyte-gated rutile TiO_2 single crystals, ACS Nano **7**, 8074 (2013).

[26] D. Okuyama, M. Nakano, S. Takeshita, H. Ohsumi, S. Tardif, K. Shibuya, T. Hatano, H. Yumoto, T. Koyama, H. Ohashi, M. Takata, M. Kawasaki, T. Arima, Y. Tokura, and Y. Iwasa, Gate-tunable gigantic lattice deformation in VO_2, Appl. Phys. Lett. **104**, 23507 (2014).

[27] X. Leng, J. Pereiro, J. Strle, G. Dubuis, A. T. Bollinger, A. Gozar, J. Wu, N. Litombe, C. Panagopoulos, D. Pavuna, and I. Božović, Insulator to metal transition in WO_3 induced by electrolyte gating, Quantum Mater. **2**, 35 (2017).

[28] N. Lu, P. Zhang, Q. Zhang, R. Qiao, Q. He, H.-B. Li, Y. Wang, J. Guo, D. Zhang, Z. Duan, Z. Li, M. Wang, S. Yang, M. Yan, E. Arenholz, S. Zhou, W. Yang, L. Gu, C.-W. Nan, J. Wu, Y. Tokura, and P. Yu, Electric-field control of tri-state phase transformation with a selective dual-ion switch, Nature **546**, 124 (2017).

[29] G. Dubuis, Y. Yacoby, H. Zhou, X. He, A. T. Bollinger, D. Pavuna, R. Pindak, and I. Božović, Oxygen displacement in cuprates under ionic liquid field-effect gating, Sci. Rep. **6**, 32378 (2016).

[30] Y. Dong, H. Xu, Z. Luo, H. Zhou, D. D. Fong, W. Wu, and C. Gao, Effect of gate voltage polarity on the ionic liquid gating behavior of $NdNiO_3/NdGaO_3$ heterostructures, APL Mater. **5**, 51101 (2017).

[31] A. M. Perez-Muñoz, P. Schio, R. Poloni, A. Fernandez-Martinez, A. Rivera-Calzada, J. C. Cezar, E. Salas-Colera, G. R. Castro, J. Kinney, C. Leon, J. Santamaria, J. Garcia-Barriocanal, and A. M. Goldman, In operando evidence of deoxygenation in ionic liquid gating of $YBa_2Cu_3O_{7-x}$, Proc. Natl. Acad. Sci. **114**, 215 (2017).

[32]   See Supplemental Material at LINK for additional information on film growth, device fabrication, in operando measurements, and complementary bulk measurements/calculations.

[33]   M. A. Torija, M. Sharma, M. R. Fitzsimmons, M. Varela, and C. Leighton, Epitaxial $La_{0.5}Sr_{0.5}CoO_3$ thin films: Structure, magnetism, and transport, J. Appl. Phys. **104**, (2008).

[34]   M. A. Torija, M. Sharma, J. Gazquez, M. Varela, C. He, J. Schmitt, J. A. Borchers, M. Laver, S. El-Khatib, and C. Leighton, Chemically driven nanoscopic magnetic phase separation at the $SrTiO_3(001)/La_{1-x}Sr_xCoO_3$ interface, Adv. Mater. **23**, 2711 (2011).

[35]   J. Gazquez, S. Bose, M. Sharma, M. A. Torija, S. J. Pennycook, C. Leighton, and M. Varela, Lattice mismatch accommodation via oxygen vacancy ordering in epitaxial $La_{0.5}Sr_{0.5}CoO_{3-\delta}$ thin films, APL Mater. **1**, 12105 (2013).

[36]   S. Kelly, F. Galli, J. Aarts, S. Bose, M. Sharma, and C. Leighton, Direct real space observation of magneto-electronic inhomogeneity in ultra-thin film $La_{0.5}Sr_{0.5}CoO_{3-\delta}$ on $SrTiO_3(001)$, Appl. Phys. Lett. **105**, 2012 (2014).

[37]   B. J. Kirby, P. A. Kienzle, B. B. Maranville, N. F. Berk, J. Krycka, F. Heinrich, and C. F. Majkrzak, Phase-sensitive specular neutron reflectometry for imaging the nanometer scale composition depth profile of thin-film materials, Curr. Opin. Colloid Interface Sci. **17**, 44 (2012).

[38]   G. Kresse and J. Hafner, Ab initio molecular dynamics for liquid metals, Phys. Rev. B **47**, 558 (1993).

[39]   G. Kresse and J. Furthmüller, Efficient iterative schemes for ab initio total-energy calculations using a plane-wave basis set, Phys. Rev. B **54**, 11169 (1996).

[40]   X. Wu, J. Walter, T. Feng, J. Zhu, H. Zheng, J. F. Mitchell, N. Biškup, M. Varela, X.

Ruan, C. Leighton, and X. Wang, Glass-like thermal conductivity induced by oxygen vacancies in nanoscale epitaxial $La_{0.5}Sr_{0.5}CoO_{3-\delta}$, Adv. Funct. Mater. In Press.

[41] Note here that a crossover from $R\bar{3}c$ to $Pm\bar{3}m$ occurs around x = 0.5 in LSCO. While minor deviations from cubic are thus possible, we simply analyze all data here in terms of the cubic structure.

[42] R. P. Haggerty and R. Seshadri, Oxygen stoichiometry, crystal structure, and magnetism of $La_{0.5}Sr_{0.5}CoO_3$, J. Phys. Condens. Matter **16**, 6477 (2004).

[43] J. Mizusaki, Y. Mima, S. Yamauchi, and K. Fueki, Nonstoichiometry of the perovskite-type oxides $La_{1-x}Sr_xCoO_{3-\delta}$, J. Solid State Chem. **80**, 102 (1989).

[44] A. Ringuedé and J. Fouletier, Oxygen reaction on strontium-doped lanthanum cobaltite dense electrodes at intermediate temperatures, Solid State Ionics **139**, 167 (2001).

[45] H. Hsu, P. Blaha, R. M. Wentzcovitch, and C. Leighton, Cobalt spin states and hyperfine interactions in $LaCoO_3$ investigated by LDA+U, Phys. Rev. B **82**, 100406 (2010).

[46] This value has been estimated in our prior work [40] to lie around 0.09 for similar films grown on LAO.

[47] As reported earlier [22], LAO(001)/LSCO films exhibit strong perpendicular magnetic anisotropy. A large (3 T) in-plane magnetic field was thus required to achieve the in-plane alignment necessary for PNR in the geometry shown in Fig. 3(a).

[48] J. Wu and C. Leighton, Glassy ferromagnetism and magnetic phase separation in $La_{1-x}Sr_xCoO_3$, Phys. Rev. B **67**, 174408 (2003).

[49] R. De Souza, Oxygen transport in $La_{1-x}Sr_xMn_{1-y}Co_yO_{3\pm\delta}$ perovskites Part I. Oxygen tracer diffusion, Solid State Ionics **106**, 175 (1998).

[50] D. A. Gilbert, A. J. Grutter, P. Murray, R. V. Chopdekar, A. M. Kane, A. L. Ionin, S. R.

Spurgeon, B. J. Kirby, B. B. Maranville, A. T. N'Diaye, A. Mehta, E. Arenholz, K. Liu, Y. Takamura, and J. A. Borchers, Ionic tuning of cobaltites at the nanoscale, Under eview.

[51] H. Jeen, W. S. Choi, M. D. Biegalski, C. M. Folkman, I.-C. Tung, D. D. Fong, J. W. Freeland, D. Shin, H. Ohta, M. F. Chisholm, and H. N. Lee, Reversible redox reactions in an epitaxially stabilized $SrCoO_x$ oxygen sponge, Nat. Mater. **12**, 1057 (2013).

FIGURE CAPTIONS

Fig. 1. (a) Device and experimental setup schematic for synchrotron X-ray diffraction on epitaxial $La_{0.5}Sr_{0.5}CoO_{3-\delta}$ films. (b) Gate-bias-(V_g)-dependent specular diffraction (00L) scans, where L is in reciprocal lattice units (r.l.u.) of the LAO substrate. (c) Change in c-axis lattice parameter (Δc_{op}, left axis) and cell volume (ΔV, right axis) with V_g. (d) Change in Scherrer thickness (Δt_s, left axis), and t_s itself (right axis), *vs.* V_g. (e) Change in film thickness from Laue fringes (Δt_f), and t_f itself (right axis), *vs.* V_g. Blue dotted lines are guides to the eye.

Fig. 2. (a) Powder X-ray diffraction patterns of *bulk* $La_{0.5}Sr_{0.5}CoO_{3-\delta}$ before and after the thermogravimetric analysis (TGA) scans shown in (b), which induce progressive reduction. The δ values from TGA are labeled on the right side of (a), and the curves are color-coordinated with (b). * denotes samples no longer in the perovskite structure, which are omitted from further analysis. (b) Reference powder diffraction pattern for cubic $La_{0.5}Sr_{0.5}CoO_3$. (c) *Bulk* TGA scans, *i.e.*, sample mass change (left axis) and conversion to δ (right axis) *vs.* temperature, for reduction in flowing N_2. (d) Change in *bulk* cell volume (ΔV) and *bulk* lattice parameter (a) as a function of δ. The maroon dotted line is a straight line fit and the solid black lines are the theoretical ΔV due to formation of oxygen vacancies (U_{Co} = 5 and 6 eV). (e) Change in δ ($\Delta\delta$) with V_g in *epitaxial films*, obtained by combining Figs. 1(c) and 2(d). The blue dashed line is a guide to the eye.

Fig. 3. (a) Device and experimental setup schematic for polarized neutron reflectometry on epitaxial $La_{0.5}Sr_{0.5}CoO_{3-\delta}$ films. (b) Reflectivity (R) *vs.* scattering vector magnitude, Q, from a 165 Å film at zero gate bias (V_g), 30 K, and 3 T. Black and red denote the non-spin-flip "R^{++}" and "R^{--}" channels, respectively, for both data (points) and the fits to the model discussed in the text (lines). (c-e) Spin asymmetry at 30 K in 3T for V_g = 0, 2, and 3 V, respectively. Solid lines

are fits to the model discussed in the text. (f) Extracted magnetization (M) depth profile at 30 K

in 3 T for V_g = 0, 2, and 3 V; $z = 0$ is the substrate/film interface.

Figure 1

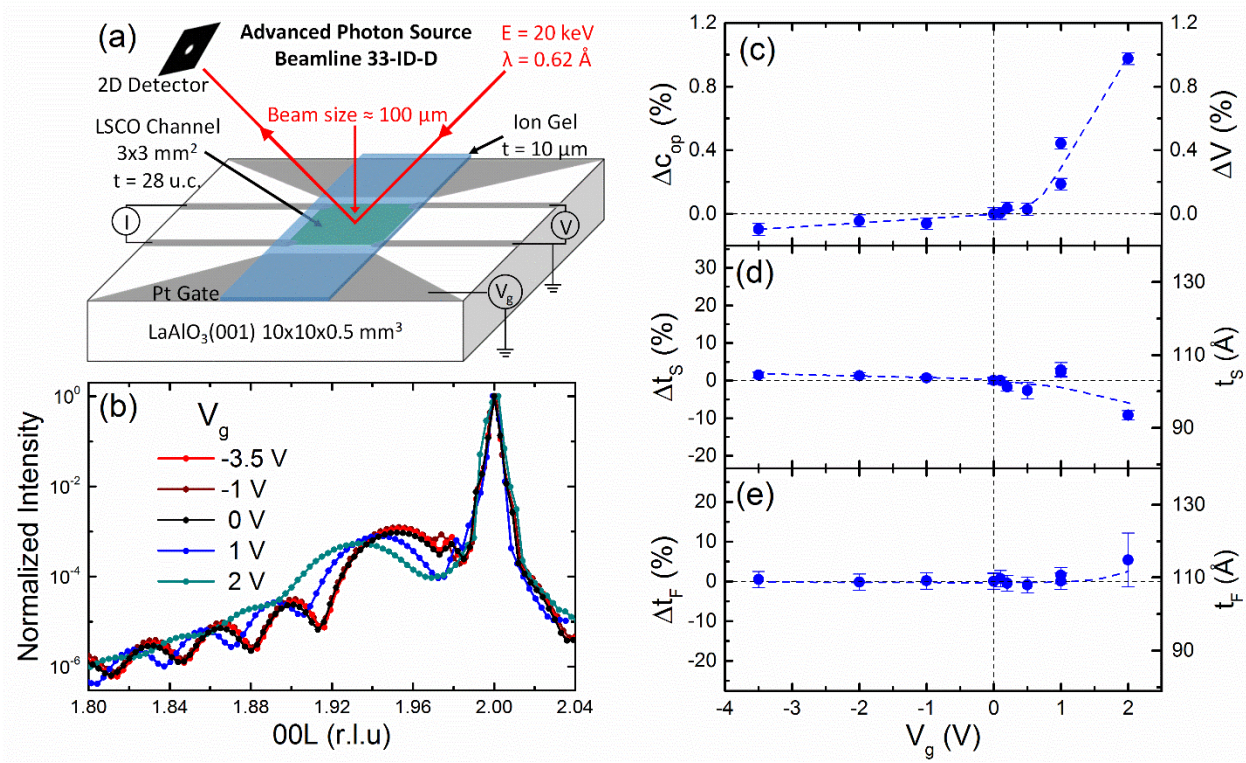**Figure 2**
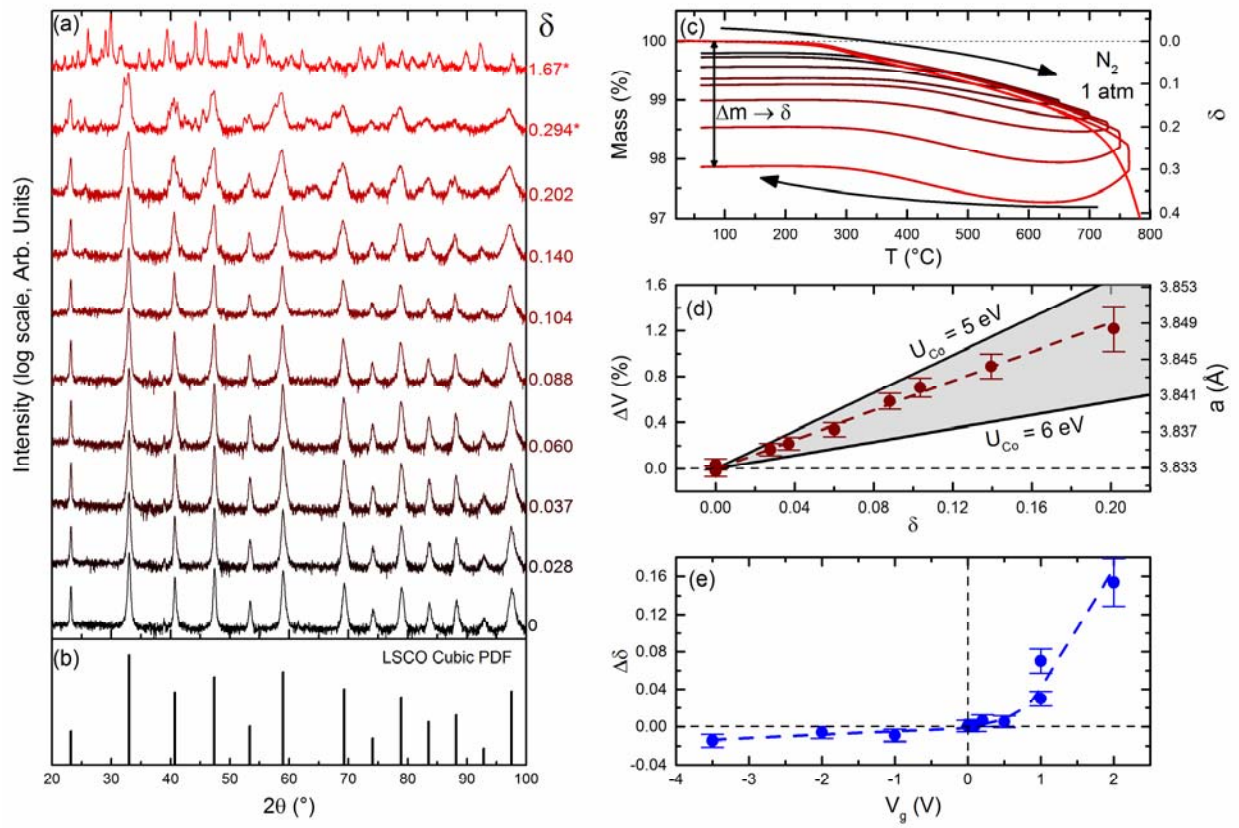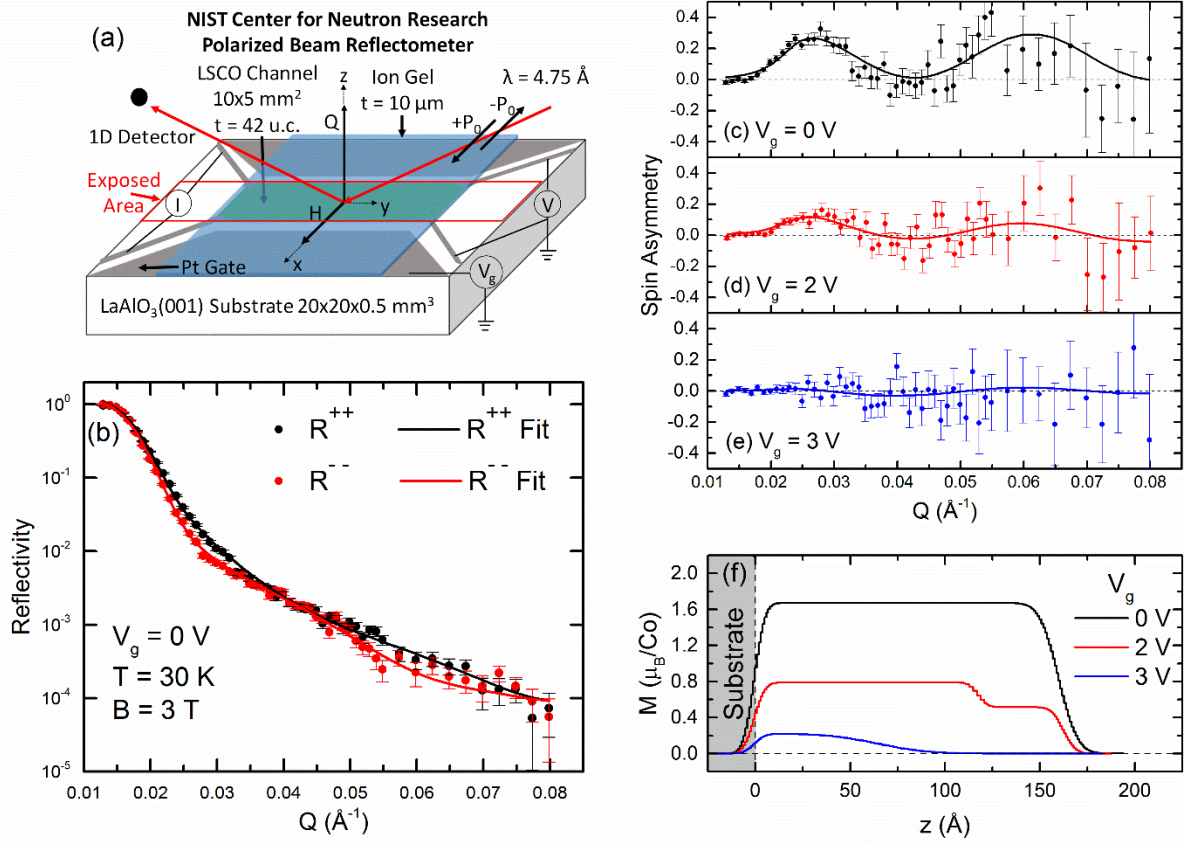
Figure 3